AGU PUBLICATIONS

Water Resources Research

RESEARCH ARTICLE
10.1002/2015WR017018

Climatic and landscape controls on water transit times and silicate mineral weathering in the critical zone

Xavier Zapata-Rios[1], Jennifer McIntosh[1], Laura Rademacher[2], Peter A. Troch[1], Paul D. Brooks[1,3], Craig Rasmussen[4], and Jon Chorover[4]

[1]Department of Hydrology and Water Resources, University of Arizona, Tucson, Arizona, USA, [2]Earth and Environmental Sciences, University of the Pacific, Stockton, California, USA, [3]Department of Geology and Geophysics, University of Utah, Salt Lake City, Utah, USA, [4]Soil, Water, and Environmental Science, University of Arizona, Tucson, Arizona, USA

Key Points:
- We quantified Effective Energy and Mass Transfer (EEMT) to the critical zone
- EEMT is tested as a controlling factor on water age and weathering from springs
- EEMT strongly correlates with water age and solutes from spring waters

Correspondence to:
X. Zapata-Rios,
xavierzapata@email.arizona.edu

Citation:
Zapata-Rios, X., J. McIntosh, L. Rademacher, P. A. Troch, P. D. Brooks, C. Rasmussen, and J. Chorover (2015), Climatic and landscape controls on water transit times and silicate mineral weathering in the critical zone, *Water Resour. Res.*, *51*, 6036–6051, doi:10.1002/2015WR017018.

Received 29 JAN 2015
Accepted 28 JUN 2015
Accepted article online 2 JUL 2015
Published online 3 AUG 2015

Abstract The critical zone (CZ) can be conceptualized as an open system reactor that is continually transforming energy and water fluxes into an internal structural organization and dissipative products. In this study, we test a controlling factor on water transit times (WTT) and mineral weathering called Effective Energy and Mass Transfer (EEMT). We hypothesize that EEMT, quantified based on local climatic variables, can effectively predict WTT within—and mineral weathering products from—the CZ. This study tests whether EEMT or static landscape characteristics are good predictors of WTT, aqueous phase solutes, and silicate weathering products. Our study site is located around Redondo Peak, a rhyolitic volcanic resurgent dome, in northern New Mexico. At Redondo Peak, springs drain slopes along an energy gradient created by differences in terrain aspect. This investigation uses major solute concentrations, the calculated mineral mass undergoing dissolution, and the age tracer tritium and relates them quantitatively to EEMT and landscape characteristics. We found significant correlations between EEMT, WTT, and mineral weathering products. Significant correlations were observed between dissolved weathering products (Na^+ and DIC), ^3H concentrations, and maximum EEMT. In contrast, landscape characteristics such as contributing area of spring, slope gradient, elevation, and flow path length were not as effective predictive variables of WTT, solute concentrations, and mineral weathering products. These results highlight the interrelationship between landscape, hydrological, and biogeochemical processes and suggest that basic climatic data embodied in EEMT can be used to scale hydrological and hydrochemical responses in other sites.

1. Introduction

The Critical Zone (CZ) is the uppermost land surface layer of the planet that extends from the base of the weathered bedrock to the top of the vegetation canopy. Within the CZ, energy and water fluxes drive coupled chemical, physical, biological, and geological processes that support life [*Brantley et al*., 2007]. Understanding the formation, evolution, and functioning of the CZ is fundamental for predicting its response to ongoing changes in climate and land cover [*National Research Council*, 2001].

Mineral weathering is a fundamental process occurring within the CZ that influences soil development and nutrient release [*White and Brandley*, 1995], as well as the buffering of acids derived from the atmosphere and biosphere [*Velbel and Price*, 2007]. Furthermore, weathering of silicate minerals impacts the global carbon cycle through the consumption of atmospheric CO_2 [*Berner et al*., 1983; *Berner*, 1995; *Maher and Chamberlain*, 2014], and the aqueous phase products of chemical weathering are determinants of the chemical composition of natural waters [*Bricker*, 1986; *Drever*, 1988]. During weathering, atmospheric CO_2 and silicate minerals are converted to alkalinity and dissolved cations. Many silicate weathering studies demonstrate that hydrologic factors, and particularly water transit time (WTT), play an important regulatory role on weathering of silicates [*Velbel*, 1993; *White et al*., 2001; *Gabet et al*., 2006; *Maher* 2010, 2011].

Water transit time (WTT) refers to the period of time between when water enters and exits the hydrologic system [*McGuire and McDonnell*, 2006]. WTT is a good indicator of the hydrologic response of a system over a period of time and provides information about flow path heterogeneity, subsurface storage capacity, water input-output fluxes, mineral weathering, and solute transport [*McGuire and McDonnell*, 2006]. Over the last decade, research efforts have focused on understanding the factors that control WTT at diverse spatial scales and in different geographic regions [*McGlynn et al*., 2003; *McGuire et al*., 2005; *Rodgers et al*., 2005; *Soulsby et al*., 2006; *Stewart et al*., 2010; *Mueller et al*., 2012, many others]. In these investigations, the role of

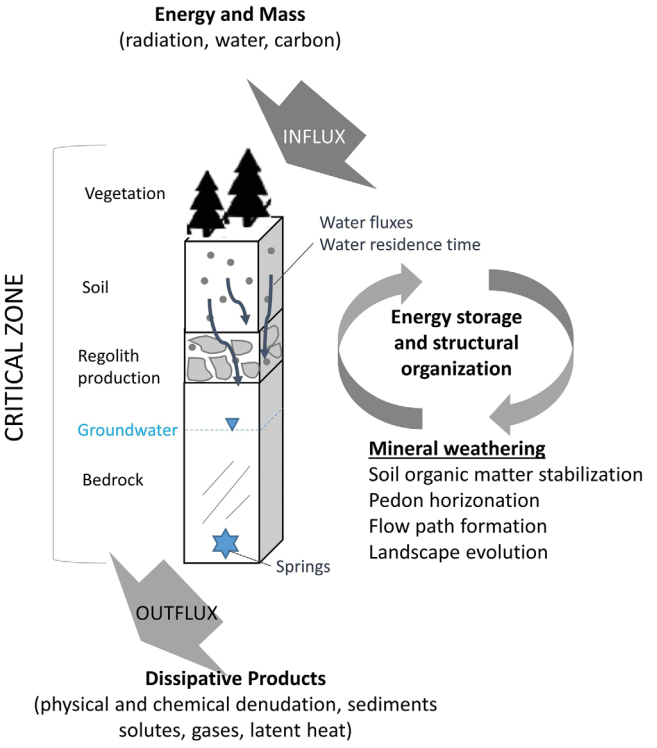

Figure 1. Conceptualization of dominant critical zone (CZ) processes [after *Chorover et al*., 2011; *Rasmussen et al*., 2011].

landscape structure, topography, soils, geology, and climate on WTT have been tested at different sites with results that have been difficult to transfer from one specific research site to others [*Vitvar et al*., 2005; *Tetzlaff et al*., 2009].

In the present study, we test the predictive power of a postulated control factor on WTT and mineral weathering derived from climatic data and based on thermodynamic concepts termed effective energy and mass transfer (EEMT) to the CZ [*Rasmussen et al*., 2011]. The CZ can be conceptualized as an open system reactor that is continually transforming energy and water fluxes (Figure 1) [*Chorover et al*., 2011; *Rasmussen et al*., 2011]. Energy and water fluxes generate internal structural organization within this reactor, driving processes such as soil organic carbon stabilization, pedon horizonation, flow path formation, and mineral weathering, among others. Dissipative products resulting from CZ internal processes leave the reactor via physical and chemical fluxes and latent heat [*Chorover et al*., 2011; *Rasmussen et al*., 2011].

Energy-based pedogenic models attempt to quantify energy fluxes to the soil system that drive mineral weathering and CZ development. Some initial work and semiquantitative approaches describing soil formation factors (climate, biota, relief, parent material, and time) were developed by *Dokuchaev* [1967], *Jenny* [1941], *Runge* [1973], and *Smeck et al*. [1983]. Later, these soil forming factors were quantified in terms of energy [*Volobuev*, 1964; *Phillips*, 2009; *Rasmussen et al*., 2005; *Rasmussen and Tabor*, 2007]. The EEMT term in particular is focused on the energy and mass transfer to the subsurface in the form of heat energy associated with effective precipitation (water in excess from evapotranspiration) (E_{ppt}) and chemical energy associated with reduced carbon compounds produced through primary production (E_{bio}). Other possible energy fluxes to the CZ such as potential energy from transport of sediments, geochemical potential of chemical weathering, external inputs of dust, heat exchange between soil and atmosphere, and others coming from anthropogenic sources are orders of magnitude smaller [*Phillips*, 2009; *Rasmussen et al*., 2011; *Rasmussen*, 2012]. EEMT is calculated from meteorological data (precipitation and air temperature) and empirical relations to predict net ecosystem exchange (NPP) based on climate (equation (1)).

$$EEMT = E_{ppt} + E_{bio} \quad (1)$$

where $E_{ppt} = \Delta T C_w P_{eff}$; $E_{bio} = NPP^* h_{bio}$; ΔT = air temperature—273 (K), C_w = specific heat of water (J kg^{-1} K^{-1}), Peff (effective precipitation) = precipitation minus evapotranspiration, NPP = net primary productivity derived from climate [*Lieth*, 1975], and h_{bio} is the specific biomass enthalpy and equivalent to 22 kJ m^{-2} m^{-1} [*Lieth*, 1975; *Phillips*, 2009]. For further details, see *Chorover et al*. [2011] and *Rasmussen et al*. [2011].

Recent research along elevation gradients in the western U.S. documented a significant correlation between EEMT and regolith depth, chemical depletion, and denudation rates and demonstrated weak to no correlations considering climatic variables alone such mean annual air temperature and mean annual precipitation [*Rasmussen et al*., 2005, 2011; *Rasmussen and Tabor*, 2007]. However, the relationship between inputs of energy into the CZ at a mountain scale (~40 km^2) and the influence on WTT and mineral weathering has not been explored previously.

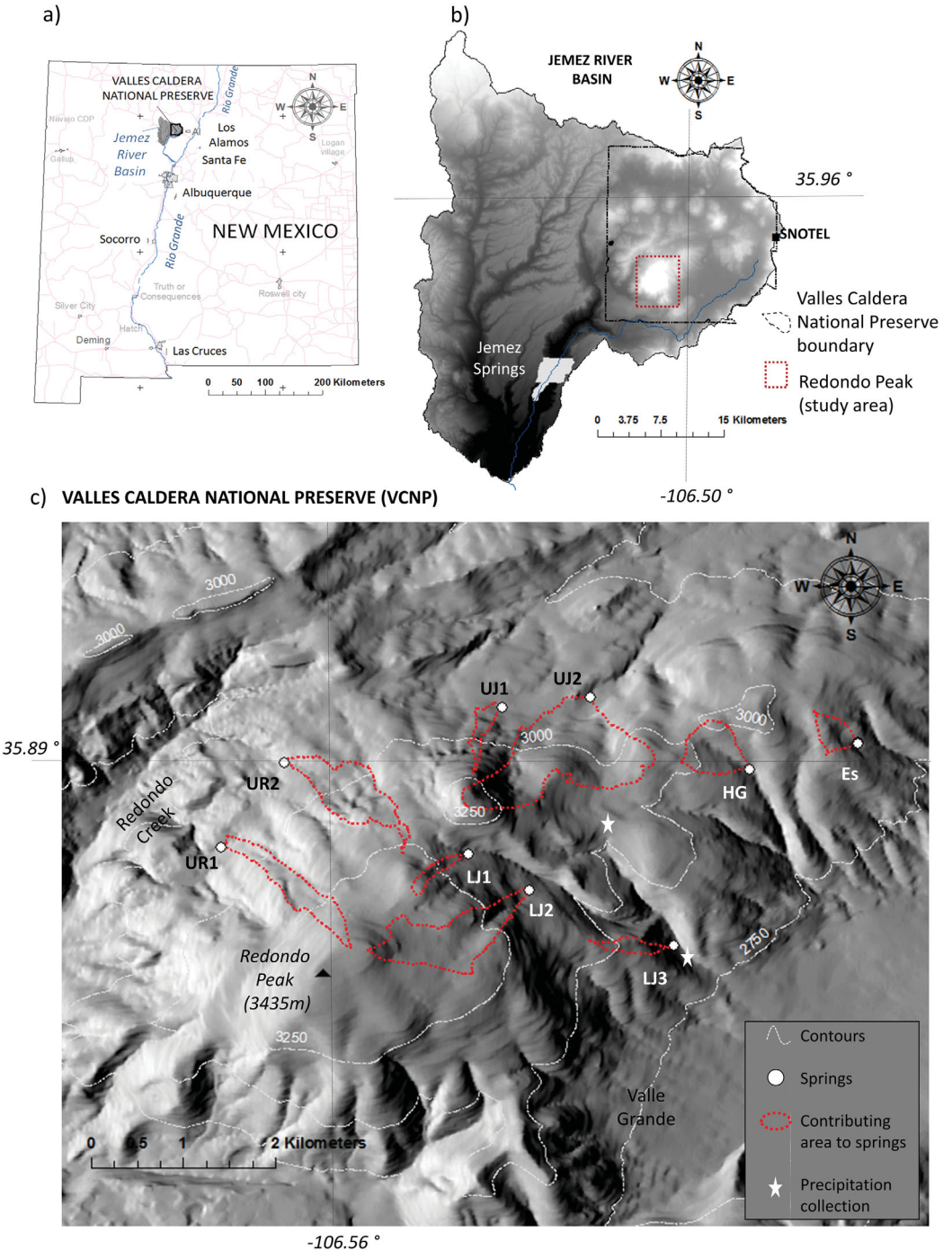

Figure 2. (a) Location of the research site in northern New Mexico, (b) location of the Valles Caldera National Preserve within the upper Jemez River Basin, and (c) Redondo peak and springs draining different terrain aspects.

Redondo Peak within the Jemez Mountains in northern New Mexico is a research site within the larger Catalina-Jemez Critical Zone Observatory (CZO) that was established to understand CZ processes [*Chorover et al.*, 2011]. Around Redondo Peak, a volcanic rhyolitic resurgent dome, headwater springs, and streams discharge along different sides of the mountain. The differences in terrain aspect around Redondo Peak create a natural gradient of energy inputs to the CZ. Previous research at this site has observed differences in solar radiation, water availability, dissolved organic carbon fluxes, and WTT across different terrain aspects of Redondo Peak [*Lyon et al.*, 2008; *Broxton et al.*, 2009; *Perdrial et al.*, 2014]. The objective of the present

Table 1. List of Springs Draining Redondo Peak Arranged From Low to High Elevation[a]

			Climate Controls				Landscape Controls						
Springs (Code)	Latitude (°)	Longitude (°)	Cos Aspect	Mean EEMT (MJ/m^2 yr)	Max EEMT (MJ/m^2 yr)	Range EEMT[b] (MJ/m^2 year)	Elevation (m)	Contributing Area ($\times 10^3$ m^2)	Mean Slope (°)	Maximum Flow Length (m)	Median Flow Length (L)[c] (m)	Median Flow Path Gradient (G)[c]	L/G[c] (m)
LJ3s	35.872	−106.529	−0.12	39.72	41.09	2.01	2816	63	16.08	896	462	0.32	1461
UR1s	35.882	−106.573	0.72	42.18	46.46	9.65	2842	287	19.94	1862	602	0.17	3489
UJ2s	35.896	−106.538	0.96	41.45	48.19	9.43	2848	1038	17.53	1482	474	0.26	1810
Es	35.892	−106.511	−0.51	38.89	40.63	2.63	2860	97	13.95	610	361	0.14	2515
UJ1s	35.896	−106.546	0.81	41.42	47.64	8.82	2876	69	15.90	851	450	0.28	1596
UR2s	35.89	−106.567	0.87	41.43	49.53	11.43	2877	404	17.23	2140	509	0.24	2111
HGs	35.889	−106.552	−0.47	40.18	41.19	1.77	2908	232	10.82	992	399	0.13	3057
LJ2s	35.877	−106.543	0.27	42.99	45.37	4.53	3070	541	12.78	1922	549	0.12	4498
LJ1s	35.881	−106.549	0.06	43.08	44.27	1.93	3170	56	13.66	766	510	0.18	2822

[a]Climate and landscape characteristics defined in a spring's contributing area.
[b]Range EEMT: Max-Min EEMT.
[c]According to *McGuire et al.* [2005].

study is to test whether EEMT or landscape characteristics are dominant controlling variables on WTT times and the main silicate weathering mass balance reactions in a terrain characterized by a relatively uniform bedrock geology.

2. Methods

2.1. Study Area

Redondo Peak lies within the Valles Caldera National Preserve (VCNP) in the Jemez Mountains of northern New Mexico (35°50′N–36°00′N; 106°24′W–106°37′W). The VCNP is a 21 km wide caldera formed by the collapse of a magma chamber approximately 1.25 Ma B.P. [*Wolff et al*., 2011]. The rim of the caldera extends to elevations above 2800 masl and encloses a basin floor that ranges in elevation between 2500 and 2750 masl. Redondo Peak, with maximum elevation of 3435 masl, is a resurgent dome formed by magma flow through ring fracture faults and is located in the center of the caldera [*Lyon et al*., 2008]. Redondo Peak is characterized by a gradient in terrain aspect that influences wind exposure, radiation, snowmelt, sublimation, evapotranspiration, and groundwater recharge [*Lyon et al*., 2008].

Several springs and first-order streams drain all sides of Redondo Peak feeding the Jemez River basin, which is a tributary of the Rio Grande River [*Ellis et al*., 1993] (Figure 2). The geology of Redondo Peak is dominated by Pleistocene aged, densely to partially welded Bandelier Tuff, and older rhyolitic and andesitic rocks associated with older volcanic events [*Goff et al*., 2006; *Wolff et al*., 2011]. Soils across the dome are generally characterized by well-drained Mollisols, Inceptisols, and Alfisols that span coarse sandy loam to clay loam textures and contain an abundance of partially to highly decomposed organic matter in surface soil horizons (http://websoilsurvey.nrcs.usda.gov/app/HomePage.htm). Vegetation at higher elevations is dominated by Spruce-fir (*Picea pungens*), ponderosa pine (*Pinus ponderosa*), aspen (*Populas tremuloides*), and gambel oak (*Quercus gambelii*); lower elevations and valley bottoms are dominated by forest meadows and grasslands [*Muldavin et al*., 2006; *Coop and Givnish*, 2007]. The semiarid climate in this region is continental in nature and highly variable. The climate is characterized by a bimodal precipitation pattern, with ∼50% of the total annual precipitation falling as snow and rain during the winter months and ∼50% falling as rainfall during the summer monsoon season [*Sheppard et al*., 2002]. According to 31 years of records (1981–2012) at the Quemazon Snowpack Telemetry (SNOTEL) station (35°55′N; 106°24′W; 2896 masl), located 5 km east from Redondo Peak, the average annual precipitation is 711 mm, and the average summer and winter temperatures are 10.7°C and −1.1°C, respectively.

2.2. Field Investigations

2.2.1. Landscape Analysis

The springs around Redondo Peak selected for this study are characterized by perennial discharge. The springs drain slopes with different aspects (orientations) at elevations above 2800 masl (Table 1). Springs with low discharge, draining the foothills or other domes in the VCNP were not considered in this analysis.

Landscape characteristics of springs investigated in this study include aspect, contributing area, water flow length, and slope gradients. Landscape characteristics were defined using a 722 km^2 airborne LiDAR flight coverage acquired July 2010 by the National Center for Airborne Laser Mapping (NCALM). The LiDAR coverage has an average point density of 9.68 points per m^2 and vertical and horizontal RMSE resolutions of 0.1 and 1.0 m, respectively. For this study, a spring's contributing area is an idealized region where energy and matter are transferred to the CZ. Within these boundaries, it is assumed that potentiometric surface follows the shape of the terrain surface [*Wörman et al*., 2007], water flow is routed and discharged into the springs, and mineral weathering transformations occur. Contributing areas from springs and topographic analysis within each basin were defined using the catchment delineation procedures from TauDEM version 5.0 (http://hydrology.usu.edu/taudem/taudem5.0/index.html, accessed May 2014) and following procedures similar to those of *McGuire et al*. [2005]. An accumulated area grid was obtained applying a multidirectional flow algorithm. Then, maximum and median flow path lengths and gradients were computed along flow lines from each cell inside the spring catchment to the spring mouth. Flow lines are not actual stream channels but rather intended to be representative of flow path lengths and gradients in the subsurface. The mean aspect of contributing areas was calculated following the methodology indicated in *Broxton et al*. [2009], as an average of the *x* and *y* composite vectors for each aspect cell. The average aspect calculated in radians was expressed as the cosine of the angle such that north-facing terrains have a value of 1 and south-facing terrains have a value of −1.

2.2.2. Effective Energy and Mass Transfer (EEMT)

The EEMT model is based on the hypothesis that soil and the larger CZ tend to self-organize to optimize the transmission of energy flowing through the system [*Rasmussen et al*., 2005; *Rasmussen and Tabor*, 2007]. This self-organization, entropy maximization, and use of energy of natural systems are described by principles of open system thermodynamics and traditional quantitative models of soil development [*Rasmussen et al*., 2005; *Kleidon et al*., 2012]. The EEMT model quantifies external energy inputs to the CZ by integrating into one single variable the climatic and biotic forcings [*Rasmussen et al*., 2005; *Rasmussen and Tabor*, 2007]. For a more detailed description and derivation of EEMT, see *Rasmussen et al*. [2005, 2011], *Rasmussen and Tabor* [2007], and *Chorover et al*. [2011]. In the present work, we used the EEMT values as quantified by *Chorover et al*. [2011] that employs a multiple linear regression model to derive EEMT from variables that exert first-order controls on photosynthesis and effective precipitation, including topographically modified temperature, precipitation, and vapor pressure deficit similar to the procedure outlined in *Rasmussen and Tabor* [2007]:

$$\begin{aligned} \mathrm{EEMT_m} = &-3.13 + 0.00879\ (\mathrm{T}+273.15) + 0.562\mathrm{PPT} + 0.03256\ (\mathrm{T}-17.65)(\mathrm{PPT}-9.0) \\ &-0.00235\mathrm{VPD} + 0.00062(\mathrm{PPT}-9.0)(\mathrm{VPD}-662) \end{aligned} \tag{2}$$

where $\mathrm{EEMT_m}$ = EEMT (MJ m^{-2}) on a monthly basis, T = air temperature (°C), PPT = precipitation (cm), and VPD = vapor pressure deficit (Pa).

Precipitation, temperature, and dew point were obtained from the PRISM Climate Group at Oregon State University (http://www.prism.oregonstate.edu/, verified May 2015) [*Daly et al*., 2008]. PRISM climate data from 2000 to 2009 were resampled to a 10 m grid and combined with a 10 m digital elevation model to include effects of topography such as slope and aspect on solar radiation and temperature [*Yang et al*., 2007]. Monthly solar radiation was computed using ArcGIS solar analysis extension (ESRI, Redlands, CA) on the 10 m digital elevation model. Dew point and locally modified temperature were converted to vapor pressure and local saturated vapor pressure, respectively [*Buck*, 1981]. Vapor pressure deficit was estimated as the difference between the saturated and actual vapor pressures. Monthly $\mathrm{EEMT_m}$ (equation (2)) was aggregated on an annual scale. Then, an average annual EEMT map for the entire Redondo Peak was calculated based on annual EEMT values from 2000 to 2009. For further details, see *Chorover et al*. [2011]. EEMT quantification may be applied across multiple spatial (e.g., pedon, catchment, and biome) and temporal (e.g., days, months, and years) scales [*Rasmussen et al*., 2011; *Chorover et al*., 2011].

2.2.3. Hydrochemistry and Stable Isotopes

Mineral weathering processes were investigated using spring water aqueous phase chemistry. This methodology examines major solute concentrations in water as products of mineral weathering reactions [*Rademacher et al*., 2001; *Anderson and Dietrich*, 2001; *Biron et al*., 1999; *Campbell et al*., 1995; *Godderis et al*., 2006; *Godsey et al*., 2009; *Hooper et al*., 1990]. Nine perennial springs were sampled monthly from 2011 to 2013

except during those winter months when sites were inaccessible. All spring samples were analyzed for pH, electrical conductivity, dissolved oxygen, and temperature in the field. Water samples for cation analysis were collected in acid-washed 250 mL high-density polyethylene (HDPE) bottles and acidified with concentrated optima grade nitric acid. Water samples for dissolved inorganic carbon (DIC) and anions were collected in 500 mL DI-washed and combusted (475°C, 4 h) amber glass bottles. Before water collection, all the bottles were rinsed three times with sample water, then filled completely to eliminate headspace and stored cool (4°C) until laboratory analysis. Water samples from springs were collected for tritium (^{3}H) analysis in duplicate 500 mL HDPE bottles during low flow conditions in the fall 2013.

Precipitation samples (snow and rainfall) were collected from 2011 to 2013 during the period of maximum snow accumulation and the monsoon season from July to September. Snow samples were collected during the winters in 2011 and 2013 from snow pits following the methodology described in *Gustafson et al.* [2010], stored in 3.78 L Ziploc bags, and maintained frozen until they were allowed to melt overnight at room temperature. Bulk rain water samples were collected weekly in two DI-washed 500 mL HDPE bottles at multiple elevations around Redondo Peak (see Figure 2 for locations of precipitation sampling). One 500 mL bottle for stable isotope analysis contained a thin layer of mineral oil to prevent water loss by evaporation. All the water samples were filtered promptly with a 0.45 μm nylon filter in the laboratory, and splits were sent to the corresponding laboratories for further analysis. In addition, this study incorporates precipitation data collected during previous studies around Redondo Peak [*Gustafson et al.*, 2010; *Broxton et al.*, 2009].

Major cations were measured by inductively coupled plasma mass spectrometry (ICP-MS) (ELAN DRC-II, Perkin Elmer, Shelton CT) at the University of Arizona Laboratory for Emerging Contaminants (ALEC). DIC samples were analyzed with a Shimadzu TOC-VCSH Carbon analyzer (Shimadzu Scientific Instruments, Columbia) in ALEC. All the water samples were analyzed for δ^{18}O with a DLT-100 Laser Spectrometer for liquid water stable isotopes with a reported instrument precision of $\pm 0.12‰$ VSMOW at the University of Arizona.

Apparent groundwater age is the elapsed time since water is isolated from the atmosphere as it enters the critical zone to the spring discharge location [*Szabo et al.*, 1996]. Apparent groundwater age was used as an indicator of integrated WTT over each spring contributing area and was calculated according to analytical solutions for a lumped-parameter piston flow model (PFM) and exponential model (EM) for a constant input tritium concentration (equations (3) and (4)) [*Zuber et al.*, 2010]. These two models are the most commonly assumed for groundwater age determination in catchments [*McGuire and McDonnell*, 2006] and define a wide range of age that bracket real age values [*Maloszewski and Zuber*, 1996]

$$C = C_o\, e^{-\lambda t} \quad \text{PFM} \tag{3}$$

$$C = \frac{C_o}{1+\lambda t} \quad \text{EM} \tag{4}$$

where C = measured tritium in springs, C_o = measured tritium in precipitation, λ = tritium decay constant (5.576×10^{-2} year^{-1}) and t = groundwater age.

Monthly tritium concentrations in precipitation at Albuquerque have been measured since 1962 and data are available as part of the Global Network of Isotopes in Precipitation (GNIP) (http://www-naweb.iaea.org/, accessed January 2014). *Eastoe et al.* [2012] observed that volume-weighted tritium concentrations in precipitation in the south west North America and specifically at Albuquerque station (70 km from field area) have remained stable, around 9.0 TU, since the early 1990s and they are considered to be similar to the local prebomb tritium concentrations in the atmosphere [*Eastoe et al.*, 2012]. Current tritium concentrations in precipitation are higher than tritium concentrations from water recharged during the nuclear weapons testing years, providing the advantage to quantify short-term transit times taking advantage of the current constant input from the atmosphere [*Eastoe et al.*, 2012; *Morgenstern et al.*, 2010; *Stewart et al.*, 2010]. A constant tritium input value in precipitation measured at the Albuquerque station was determined from 1992 to 2005 based on weighted tritium concentrations using snow water equivalent (SWE) data from the Quemazon station. Groundwater is primarily recharged around Redondo Peak during the winter season [*Lyon et al.*, 2008; *Molotch et al.*, 2009]; therefore, groundwater recharge variations were considered proportional to

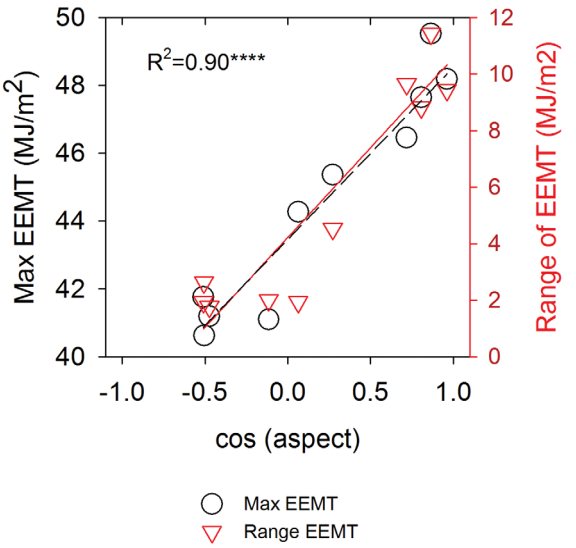

Figure 3. Maximum and range (maximum-minimum) of EETM values versus mean aspect within springs' contributing areas (***$p \leq 0.001$; ****$p \leq 0.0001$). There is no a statistically significant relationship between mean aspect and mean EEMT ($R^2 = 0.31$; $p > 0.1$).

changes in SWE [*Manning et al.*, 2012]. Tritium samples from springs were analyzed by liquid scintillation counting in a Quantulus 1220 liquid scintillation counter with a 0.7 TU detection limit following an eightfold electrolytic enrichment at the University of Arizona Environmental Isotope Laboratory. Uncertainties in the age calculation were assessed as indicated in equation (5), following procedures outlined in *Scanlon* [2000] and *Bevington and Robinson* [1992].

$$\sigma_t = \left[\left(\frac{\partial_t}{\partial_{Co}} \right)^2 \sigma_{Co}^2 + \left(\frac{\partial_t}{\partial_C} \right)^2 \sigma_C^2 \right]^{0.5} \quad (5)$$

where σ_t is uncertainty in age calculation, and σ_{Co} and σ_C are the uncertainties in the tritium measurements in precipitation and at the springs, respectively.

In addition, a quantitative mineralogical analysis was carried out on unweathered Bandelier Tuff and rhyolite rock samples. Mineral composition was determined by quantitative X-ray diffraction on random powder mounts using a PANanalytical X'Pert PRO-MPD X-ray diffraction system at the Center for Environmental Physics and Mineralogy (CEPM) at the University of Arizona [*Vazquez-Ortega et al.*, 2015].

The chemical data were used in geochemical models MINTEQA2 and NETPATH to investigate saturation indices, chemical reactions during mineral weathering, and the mass of minerals dissolving and precipitating along flow paths. MINTEQA2 is an equilibrium speciation model that calculates the equilibrium mass distribution among dissolved and adsorbed species and multiple solid phases [*Allison et al.*, 1991]. NETPATH is a model for simulating net geochemical reactions and calculating the mass balance reactions between an initial and final water along a hydrologic flow path [*Plummer et al.*, 1994]. Precipitation chemistry was corrected for evaporative concentration of solutes based on the assumption that increases in Cl^- were entirely a result of evapotranspiration [*Rademacher et al.*, 2001; *Burns et al.*, 2003]. Precipitation chemistry, corrected for evapotranspiration, was assumed as the initial preweathering composition and the chemistry from spring discharge was used as the final postweathering composition. Information on mineral phases and their stoichiometry was based on rock mineralogical analysis. NETPATH calculates the mass of minerals per kilogram of water that

Table 2. Chemical Composition of Precipitation and Springs[a]

Water Samples Code	Number of Samples	Temperature (°C)	EC (μS/cm)	pH (umol/L)	DIC (umol/L)	Ca^{2+} (umol/L)	Na^+ (umol/L)	Mg^{2+} (umol/L)	K^+ (umol/L)	Si (umol/L)	Cl^- (umol/L)	NO_3 (umol/L)-	SO_4^- (umol/L)	$\delta_{18}O$ (‰)
Snow	40			5.69	0.09 (0.1)	<5.0	2.43 (3.4)	1.54 (1.1)	<5.0	2.8 (5.4)	18.8 (16.2)	16.5 (31.9)	8.7 (13.8)	−15.0 (2.50)[b]
Rainfall	60			6.32	0.19 (0.2)	10.0 (13.5)	4.99 (4.5)	3.0 (3.4)	<5.0	2.3 (3.4)	14.6 (15.8)	12.4 (9.78)	8.2 (8.0)	−6.2 (2.90)[b]
Es	5	13.1 (3.9)	47.6 (1.6)	6.5	0.3 (0.03)	155.2 (23.5)	89.6 (3.2)	23.0 (2.0)	30.3 (23.0)	449.8 (172.2)	37.2 (12.1)	51.9 (23.8)	50.9 (7.5)	−12.7 (0.03)
HGs	9	10.6 (3.9)	37.7 (16.6)	6.2	0.33 (0.03)	139.2 (50.6)	109.6 (13.9)	32.5 (5.4)	17.4 (14.1)	447.6 (229.8)	34.1 (10.6)	38.6 (17.7)	50.4 (16.8)	−12.8 (0.21)
LJ1s	7	9.6 (3.1)	52.3 (9.6)	6.9	0.3 (0.13)	111.7 (27.1)	85.4 (10.8)	22.0 (7.1)	43.7 (20.7)	431.9 (73.7)	33.2 (20.2)	5.8 (0.8)	41.4 (30.4)	−13.1 (0.51)
LJ2s	14	7.7 (0.9)	60.9 (11.7)	7.4	0.36 (0.07)	139.4 (32.0)	139.3 (13.9)	19.9 (4.9)	23.8 (24.2)	276.4 (145.3)	20.0 (18.5)	14.8 (5.3)	25.0 (3.0)	−13.2 (0.10)
LJ3s	13	5.6 (0.6)	38.1 (9.0)	6.6	0.38 (0.1)	144.9 (46.6)	122.4 (7.1)	24.6 (7.9)	21.8 (10.4)	371.3 (186.4)	17.6 (6.8)	20.4 (10.9)	36.4 (19.6)	−12.8 (0.16)
UJ1s	5	9.8 (3.0)	56.2 (9.8)	6.5	0.41 (0.11)	135.7 (21.1)	143.8 (12.4)	20.2 (2.1)	9.7 (4.8)	237.8 (95.1)	19.8 (4.9)	42.3 (15.9)	33.0 (13.4)	−12.5 (0.06)
UJ2s	8	7.1 (0.4)	78.8 (5.5)	7.1	0.59 (0.05)	226.9 (71.3)	212.1 (21.4)	45.9 (4.9)	16.3 (11.4)	473.2 (140.2)	19.6 (3.4)	20.0 (6.3)	57.7 (28.0)	−12.9 (0.03)
UR1s	6	11.5 (7.4)	62.6 (6.2)	6.4	0.55 (0.12)	232.3 (35.5)	148.1 (15.0)	28.4 (6.7)	13.0 (9.3)	232.1 (164.4)	22.7 (21.6)	12.0 (4.7)	30.9 (7.1)	−12.4 (0.07)
UR2s	7	12.4 (2.3)	60.6 (7.3)	6.6	0.65 (0.26)	193.9 (35.1)	197.6 (38.9)	18.6 (6.9)	13.7 (14.3)	296.4 (170.3)	12.8 (4.2)	35.2 (17.7)	29.0 (13.0)	−12.1 (0.16)

[a]Mean; standard deviation in parenthesis.
[b]Including data from *Broxton et al.*, 2009 and *Gustafson et al.*, 2010.

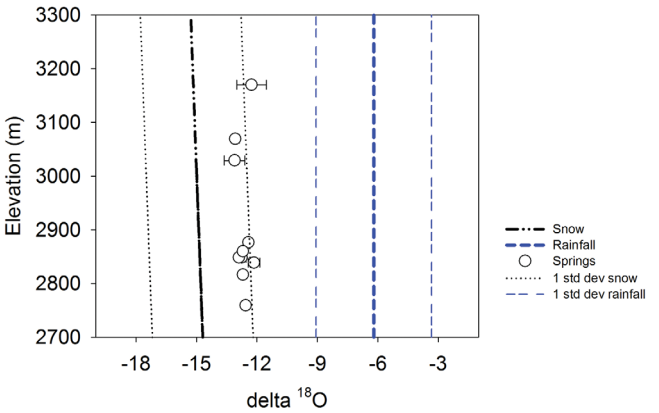

Figure 4. δ^{18}O values of precipitation and springs relative to elevation.

dissolve or precipitate along the flow path in every possible combination of the selected phases that accounts for the observed changes in water chemistry [*Plummer et al.*, 1994]. The chemical evolution and mass balance calculated by NETPATH between an initial and final water composition is assumed to only occur along flow paths [*Plummer et al.*, 1994; *Rademacher et al.*, 2001].

Finally, the estimations of EEMT, aspect and landscape characteristic in each contributing area of the springs were compared to the mean base cations concentrations and dissolved inorganic carbon concentrations, WTT, and mineral weathering dissolution measured at the springs.

3. Results

3.1. Landscape Analysis

The selected springs drain different aspects of Redondo Peak at elevations between 2816 and 3170 m. Contributing areas of springs vary in size from 56 to 1038 ($\times 10^3$ m^2) and their mean cosine angle covers a wide range of aspects from −0.5 south to 0.96 north. The mean slope of contributing areas ranges between 10° and 20°, and the median water flow path length ranges from 360 to 600 m with a median gradient between 0.12 and 0.32 (Table 1).

3.2. Quantification of Effective Energy and Mass Transfer (EEMT)

An annual EEMT map (MJ m^{-2} yr^{-1}) for the entire VCNP is presented in *Chorover et al.* [2011] (Figure 2e). EEMT values for the Redondo Peak region vary between 22 and 59 MJ m^{-2} yr^{-1}. A visual inspection of the map shows large EEMT values above 30 MJ m^{-2} yr^{-1}on Redondo Peak and low EEMT values below 30 MJ m^{-2} yr^{-1} along areas shaded by topography such as Redondo Creek in the southwestern part of Redondo. Mean, maximum, and the range of EEMT (maximum – minimum EEMT) within contributing areas of springs vary from 39 to 43, 40 to 50, and 1.8 to 11.4 MJ m^{-2} yr^{-1}, respectively (Table 1). The mean aspect of a spring contributing area positively correlates with mean EEMT ($R^2 = 0.31$; $p > 0.1$), maximum EEMT ($R^2 = 0.90$; $p < 0.0001$), and the range of EEMT ($R^2 = 0.82$; $p = 0.0007$) (Figure 3). Based on the maximum EEMT versus aspect relationship, north-facing slopes receive up to 25% more EEMT than south-facing slopes (Figure 3).

3.3. Precipitation Water Stable Isotopes

The stable isotope composition of precipitation exhibits a seasonal pattern with enriched δ^{18}O values during the monsoon season and depleted values during the winter. There is an altitudinal isotopic effect observed in winter precipitation (1‰ decrease/increase in δ^{18}O per 1000 m elevation change), but no corresponding effect observed for summer precipitation [*Broxton et al.*, 2009; *Adams et al.*, 1995]. The weighted mean and standard deviation of the δ^{18}O values of the snow and rainfall samples are -15.0 ± 2.5‰ and -6.2 ± 2.9‰, respectively. Isotopic variability of the spring waters is considerably more damped and lies between values from snow and monsoon rainfall (Table 2). δ^{18}O values from snow, rainfall and springs indicate that the springs are predominantly recharged by spring snowmelt (Figure 4), which is consistent with findings from previous research demonstrating that the source of subsurface hydrologic recharge in the VCNP is snowmelt dominated [*Broxton et al.*, 2009].

3.4. Spring Water Major Ion Chemistry

Spring waters are dominated by Ca^{2+}, Na^+, Si, and HCO_3^- ions (Table 2). Dissolved inorganic carbon (DIC) concentrations strongly correlate with the products of silicate weathering, including the sum of all base cations ($R^2 = 0.92$; $p < 0.0001$) and Na^+ concentrations ($R^2 = 0.86$; $p = 0.001$) (Figure 5a). Figures 5b–5d

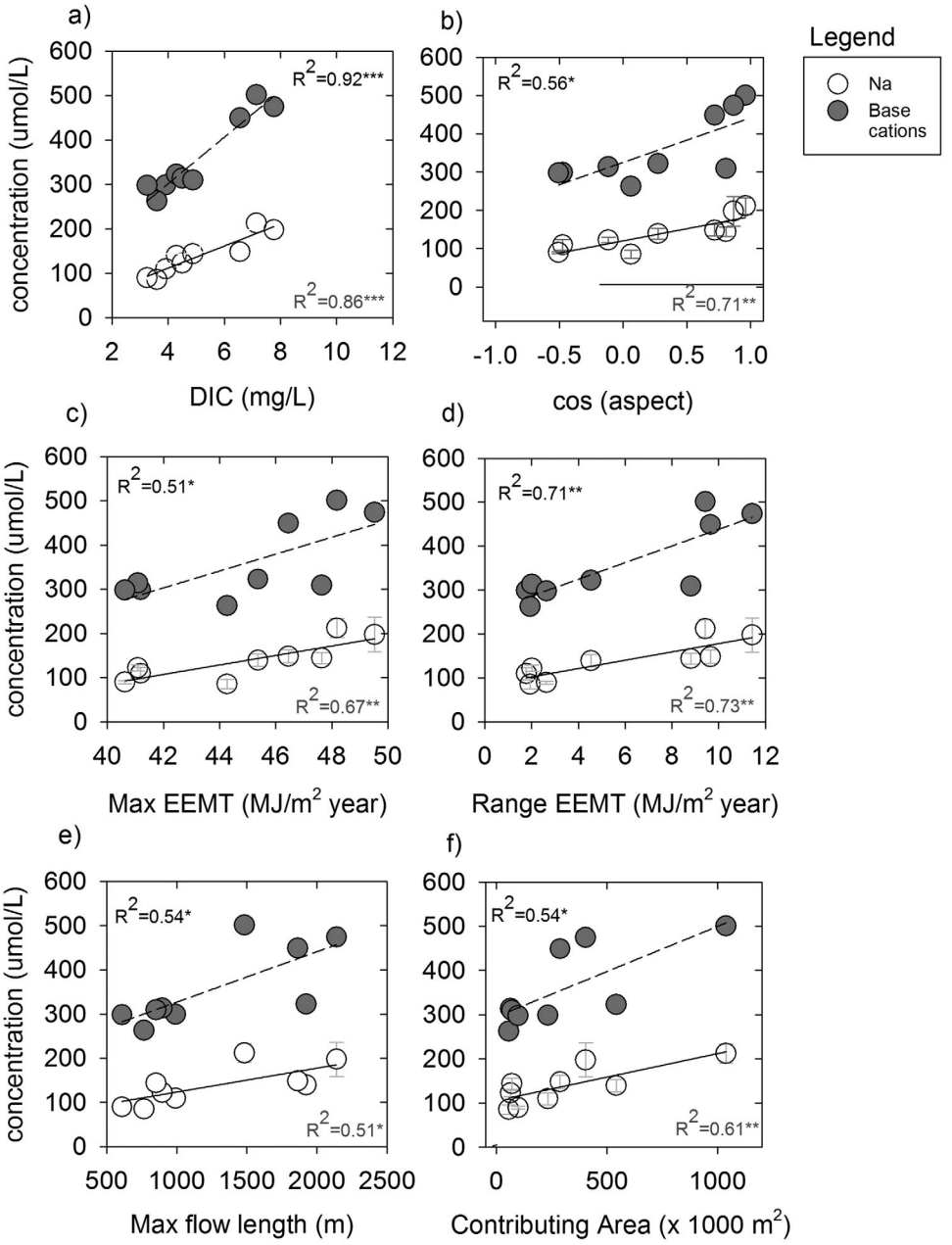

Figure 5. Concentrations of base cations, Na^+, and DIC in spring water versus EEMT (Range and Maximum EEMT values estimated for each contributing area) and landscape characteristics (Max flow length and contributing area). Statistical significance (*$p \leq 0.05$; **$p \leq 0.01$; ***$p \leq 0.001$).

indicate significant correlations between all base cations and Na^+ concentrations versus aspect, maximum, and range of EEMT. Sodium release was used as a proxy for silicate weathering because Na^+ accumulation in biomass and secondary mineral structures can be considered negligible [*White and Brantley*, 2003; *Lybrand and Rasmussen*, 2014] as also supported by saturation indices calculated for water samples in the present study. Na^+ is the cation that shows the strongest correlations with aspect and EEMT. Water with higher concentrations of solutes is found along north-facing slopes ($R^2 = 0.56$; $p < 0.05$), which are characterized in this study by higher EEMT values ($R^2 = 0.51$; $p < 0.05$). Maximum flow path length and contributing area are the only two landscape characteristics that show statistically significant correlations with both base cations and Na^+ concentrations (Figures 5e and 5f). Larger concentrations of base cations are observed in springs with longer flow paths ($R^2 = 0.54$; $p < 0.05$) and larger contributing areas ($R^2 = 0.54$;

Table 3. Apparent Age Calculated for a Constant Input Tritium Concentration in Precipitation According to Analytical Solutions for a Lumped-Parameter Piston Flow Model (PFM) and Exponential Model (EM)

		Age (Years)		σ_t[b]	
Spring	Tritium (TU) (σ_C[a])	PFM	EM	PFM	EM
Es	7.9 ± 0.39	1.5	1.6	1.7	0.2
HGs	6.0 ± 0.43	6.5	7.8	1.9	0.8
LJ1s	5.6 ± 0.39	7.7	9.6	1.9	1.0
LJ2s	5.7 ± 0.42	7.4	9.1	2.0	1.0
LJ3s	6.2 ± 0.37	5.9	6.9	1.8	0.7
UJ1s	5.6 ± 0.43	7.7	9.6	2.0	1.1
UJ2s	5.4 ± 0.38	8.3	10.6	1.9	1.1
UR1s	5.9 ± 0.41	6.8	8.2	1.9	0.9
UR2s	5.1 ± 0.40	9.4	12.3	2.0	1.4

[a]Lab reported error.
[b]Water age uncertainty.

$p < 0.05$). As indicated in Table 4, mean EEMT and other landscape variables, such as mean elevation, mean slope, median flow path length (L), median flow path slope (G), and L/G are poor predictors of both base cations and Na^+ concentrations.

3.5. Water Transit Times

A concentration of 8.6 TU in precipitation (error $\sigma_{Co} = 0.7$ TU) was used for apparent age calculations. Tritium concentrations measured at the springs ranged from 5.1 to 7.9 TU (Table 3). Water apparent age in the springs ranged from 1.5 to 9.4 years according to the PFM and from 1.6 to 12.3 according to the EM. Table 4 shows significant relations between terrain aspect versus tritium concentrations ($R^2 = 0.74$; $p < 0.01$) and maximum EEMT versus apparent water age (Figure 6). Similarly, water samples in springs with longer WTT had correspondingly higher Na^+ concentrations (Figure 6).

3.6. Bedrock Composition and Mass Balance Analysis

Mineralogical analyses of Redondo Peak bedrock samples indicate predominance of primary phases sanidine, oligoclase, anorthoclase, and quartz, accompanied by minor minerals, including apatite, hematite, zircon, titanite, ilmenite, and faujasite (Table 5) (for detailed mineralogy see *Vazquez-Ortega et al.* [2015]). Spring waters are undersaturated with respect to silica, halite, calcite, gypsum, sanidine, and albite, but saturated to supersaturated with respect to secondary minerals gibbsite, goethite, hematite, and kaolinite (Table 6). Saturation index results from MINTEQA2 were used to select mineral phases for inclusion in NETPATH (sanidine, oligoclase, anorthoclase, quartz, calcite, kaolinite, gypsum, gibbsite, goethite, albite, biotite, albite, hornblende, halite, and CO_2 gas). NETPATH then generated 64 models that produced a mass balance between the input waters (evaporated snow chemistry) and spring discharge using the selected phases. Figure 7 shows the mean and standard deviation of the mineral mass balance from the 64 possible combinations of mineral phases that explain the chemistry observed for two springs with contrasting aspect. The results from NETPATH are consistent with the results from MINTEQA2 and indicate for all the springs the same minerals dissolving and precipitating. The model predicts that gibbsite, goethite, hematite, and kaolinite precipitate and all the remaining minerals dissolve along the hydrologic flow paths. Mineral dissolution calculated using NETPATH is strongly correlated with aspect and EEMT; the highest mineral weathering dissolution amounts were observed in springs discharging north-facing aspects (Figure 8).

Table 4. Linear Regression Between Climate/Landscape Variables and Solutes, Mineral Dissolution, and Tritium Concentrations

		R^2				
		HCO3 (umol/L)	Na+ (umol/L)	Base Cations (umol/L)	Anorthoclase[a] (mmol/L)	Tritium (TU)
Climate	Cosine aspect	0.71**	0.71**	0.56*	0.71**	0.74**
	Max EEMT (MJ/m^2)	0.67**	0.67**	0.51*	0.76***	0.78***
	Range EEMT (MJ/m^2)	0.82***	0.73**	0.71**	0.85***	0.45*
	Mean EEMT (MJ/m^2)	0.04	0.04	0.03	0.10	0.49*
Landscape	Mean Elevation (m)	0.18	0.16	0.22	0.10	0.06
	Contributing Area (m^2)	0.38	0.61*	0.54*	0.27	0.19
	Mean slope (°)	0.59*	0.37	0.56*	0.42	0.21
	Max flow path length (m)	0.57*	0.51*	0.54*	0.69**	0.38
	Median flow path length, L (m)[b]	0.24	0.13	0.18	0.25	0.47*
	Median flow path slope, G[b]	0.17	0.19	0.08	0.11	0.15
	L/G (m)[b]	0.05	0.06	0.02	0.02	0.00

[a]Anorthoclase dissolution determined by NETPATH. Same R^2 and p values were found for sanidine and oligoclase.
[b]According to *McGuire et al.* [2005].
Statistical significance
*$p \leq 0.05$.
**$p \leq 0.01$.
***$p \leq 0.001$.

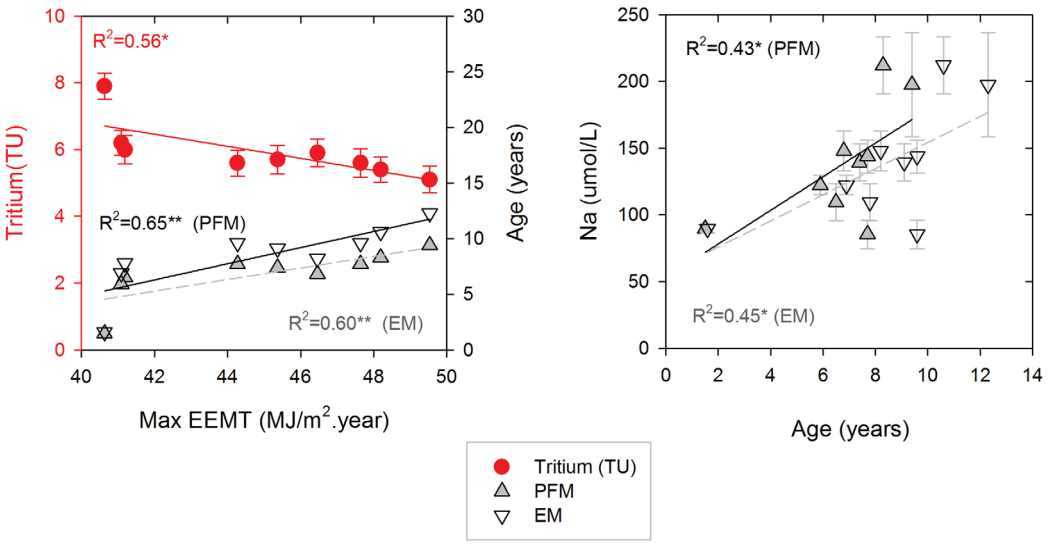

Figure 6. (left) Max EEMT versus tritium concentration and apparent age. (right) Apparent age versus Na^+ concentrations. Statistical significance (*$p \leq 0.05$; ** $p \leq 0.01$).

4. Discussion

Extensive work has been done on WTT and mineral weathering [*Rademacher et al.*, 2001, 2005; *Buttle et al.*, 2001; *Morgenstern et al.*, 2010; *Burns et al.*, 2003, many others] but no study has investigated before energy and mass fluxes quantified using EEMT on both WTT and mineral weathering. This study provides evidence that EEMT modeling can predict, at a large scale (~40 km^2), measured components of CZ hydrologic and aqueous geochemical function, such as WTT and incongruent weathering of silicates. The predictive power of EEMT observed in this high-elevation subhumid region is consistent with previous work that demonstrated in the western U.S. strong relations between EEMT and Si fluxes from granitoid watersheds, soil carbon content, pedon depth, clay content, chemical indexes of alteration [*Rasmussen et al.*, 2005, 2011]. In the study by *Rasmussen et al.* [2011], EEMT was the best predictor of pedogenic indices in contrast to weak to no correlations when mean annual temperature and precipitation alone were compared to the same pedogenic indices. Although, EEMT data are available and have been quantified across the continental U.S. and entire world [*Rasmussen and Tabor*, 2007; *Rasmussen et al.*, 2011], EEMT predictability on WTT and weathering still needs to be investigated in other humid and tropical regions.

North-facing slopes were characterized in this study with higher EEMT values (Figure 3). Lower temperatures and vapor pressure deficits in north-facing slopes (equation (2)) are the main drivers of the higher EEMT quantified in north-facing terrains (Figure 3). Since, EEMT is a variable that combines the energy associated with water and reduced carbon flux, higher EEMT values along north-facing terrains are consistent with site observations of greater water availability in the northern part of Redondo Peak [*Zapata-Rios et al.*, 2012, *Zapata-Rios*, 2015], longer WTT along north-facing slopes [*Broxton et al.*, 2009, and this study], and higher soluble organic carbon effluxes from catchments draining north-facing aspects [*Perdrial et al.*, 2014]. The results of this investigation are also consistent with laboratory and field studies that have demonstrated that weathering of silicates increase with WTT [*Velbel*, 1993; *Gabet et al.*, 2006; *Maher*, 2010, 2011; *White et al.*, 2001; *Burns et al.*, 2003; *Rademacher et al.*, 2001, 2005].

Table 5. Chemical Composition of the Most Abundant Minerals in the Valles Caldera Rhyolite (See *Vazquez-Ortega et al.* [2015] for Details)

Rhyolite	Chemical Formula
Sanidine	$K_{0.36}\ Na_{0.54}\ Al_{1.02}\ Si_{2.99}O_8$
Anorthoclase	$Na_{0.70}\ K_{0.23}\ Al_{1.05}\ Si_{2.94}\ O_8$
Oligoclase	$Na_{0.69}\ Ca_{0.24}\ Al_{1.23}\ Si_{2.76}\ O_8$
Quartz	SiO_2
Minor minerals	Apatite, Hematite, Zircon, Titanite, Ilmenite, and Faujasite

The methodology to estimate EEMT based on average climate data as presented in this study was validated with empirical estimations of EEMT at the catchment scale in 86 catchments across the U.S., showing a significant linear correlation between modeled and empirical EEMT values [*Rasmussen and Gallo*, 2013]. Empirical estimations of EEMT were calculated based on catchment scale estimations of base flow fluxes and net primary productivity derived from

Table 6. Mineral Saturation Index Log [IAP/K_{so}] Estimated With MINTEQA2[a]

Spring Code / Sample ID	Log K[b]	UR1s NMS1234	UR2s NMS1235	UJ1 NMS1237	UJ2s NMS1236	Es NMS1240	LJ1s NMS1230	LJ2s NMS1229	LJ4s NMS1238	HGs NMS1241
SiO_2	−2.71	−0.55	−0.61	−0.64	−0.52	−0.65	−0.43	−0.62	−0.66	−0.39
GIBBSITE	8.77	1.98	0.44	1.79	0.35	0.71	1.33	0.27	0.66	0.35
GOETHITE	0.50	4.94	4.75	4.19	5.21	4.40	5.15	4.65	3.74	4.02
HEMATITE	−4.00	12.19	11.82	10.69	12.73	11.11	12.61	11.61	9.78	10.36
NaCl	1.58	−10.29	−10.34	−10.17	−9.98	−9.89	−10.24	−10.23	−9.97	−10.08
CALCITE	−8.48	−1.89	−2.11	−2.85	−1.56	−2.50	−1.70	−2.12	−2.08	−2.49
GYPSUM	−4.85	−3.70	−3.89	−3.92	−3.06	−3.48	−3.07	−3.86	−3.24	−3.35
KAOLINITE	5.73	6.66	3.53	6.11	3.54	4.62	5.69	3.18	3.91	3.82
SANIDINE	1.06	−128.24	−117.43	−128.38	−131.30	−128.80	−129.65	−133.14	−140.43	−130.94
ALBITE	2.59	−85.35	−79.77	−84.70	−87.60	−85.64	−86.57	−89.02	−92.52	−86.92

[a]Note—Mineral reactions: $SiO2SiO_2 + 2H_2O = H_4SiO_4$; Gibbsite: $Al(OH)_3 + 3H^+ = Al^{+3} + 3H_2O$; Goethite: $FeOOH + 3H^+ = Fe^{+3} + 2H_2O$; Hematite: $Fe_2O_3 + 6H+ = 2Fe^{+3} + 3H_2O$; NaCl: $NaCl = Na^+ + Cl$; Calcite: $CaCO_3 = Ca^{+2} + CO^{3}_{-2}$; Gypsum: $CaSO_4{:}2H_2O = Ca^{+2} + SO_4^{-2} + 2H_2O$; Kaolinite: $Al_2Si_2O_5(OH)_4 + 6H^+ = 2Al^{+3} + 2H_4SiO_4 + H_2O$; Sanidine: $KAlSi_3O_8 + 4H_2O + H^+ = Al^{3+}\ K^+ + 3H_4SiO_4$; Albite: $NaAlSi_3O_8 + 4H^+ + 4H_2O = Na^+ + Al^{+3} + 3H_4SiO_4$.

[b]MINTEQ database.

remote sensing data. This study indicates that metrics of mineral weathering are correlated with the range and maximum values of EEMT distributed over the catchment contributing to spring discharge. The observation that mean EEMT showed less predictive power is consistent with the concept of subcatchment "hot spots" contributing disproportionately to a given catchment discharge. The fact that EEMT is not uniformly distributed across a catchment, and that it exhibits strong topographic variation from effects of aspect and topographic convergence of hydrologic flow, particularly in water limited systems, has led to inclusion of such landscape structural parameters into more recent versions of the EEMT calculation than the one employed in the current study [*Rasmussen et al.*, 2015]. This new approach for EEMT estimation could be employed in future analyses to understand why the range and maximum EEMT values are better predictors than the mean EEMT.

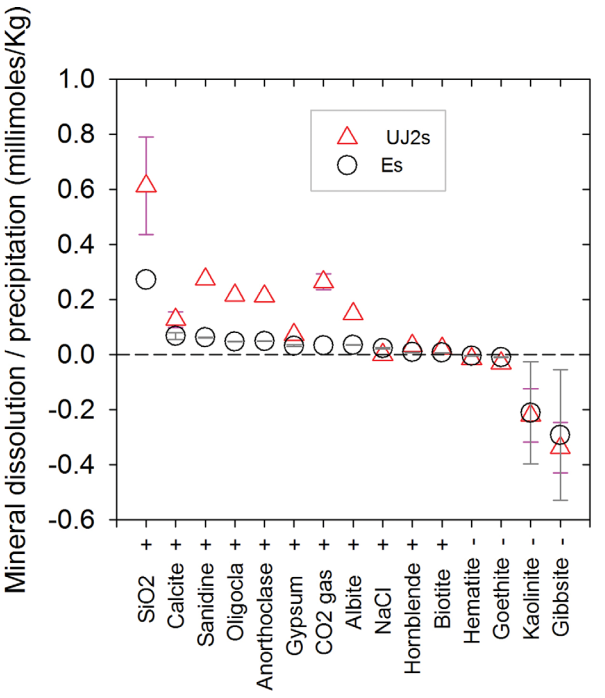

Figure 7. Mineral dissolution (plus) and precipitation (minus) for a north aspect draining (UJ2s) and south aspect draining (Es) spring. Symbols represent mean mineral dissolution and precipitation, and error bars represent 1 standard deviation from 64 mass balance models checked with NETPATH. The mass balance models determined by NETPATH represent every possible geochemical mass balance reaction between the initial and final water given a set of chemical constrains and phases.

Aqueous phase base cation concentrations (and Na^+ in particular) around Redondo Peak show strong correlations with dissolved inorganic carbon and WTT. Saturation indices (SI) provide evidence that Na^+ is behaving quite conservatively in this system, therefore, the increase in concentrations with increase in WTT can be attributed to primary mineral weathering reactions. Chemical formulae of supersaturated secondary phases also indicate that secondary mineral formation does not provide a sink for Na^+, which is also supported by a previous geochemical study around Redondo, where Na^+ was identified as a conservative tracer and used in an end-member mixing analysis [*Liu et al.*, 2008b]. *Liu et al.* [2008a, 2008b] observed that groundwater contributions dominate runoff generation throughout the year around Redondo Peak, with limited contributions from overland flow and shallow subsurface flow. In addition, base cation concentrations in surface water

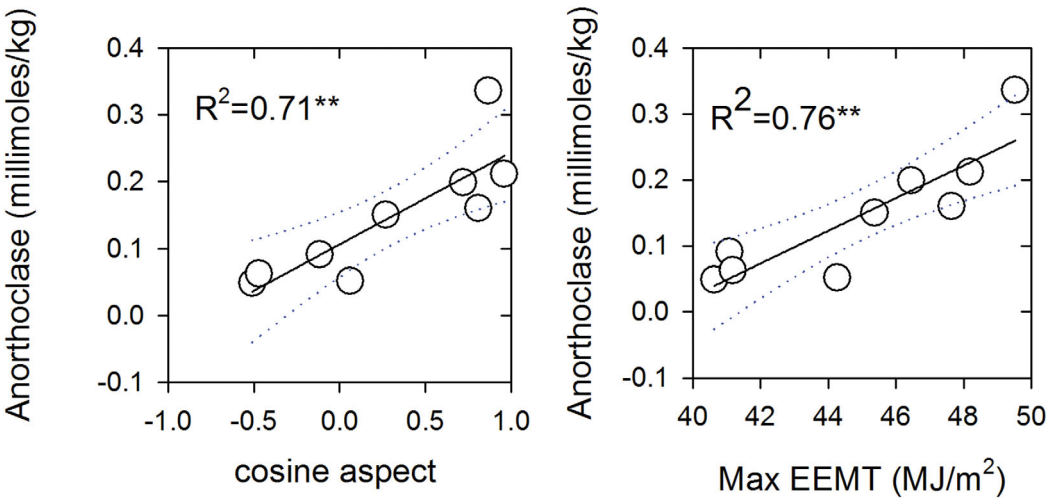

Figure 8. Dissolution of Anorthoclase estimated using NETPATH [*Plummer et al*., 1994] versus aspect and max EEMT. Statistical significance ($^{**}p \leq 0.01$).

draining Redondo Peak exhibit chemostatic behavior, which suggests a constant source of water supply to surface water, likely from a well-mixed groundwater reservoir [*Porter*, 2012; *Perdrial et al*., 2014]. Moreover, dissolved organic carbon (DOC) concentrations measured in the springs and first-order springs are significantly lower than DOC concentrations from soil waters during base flow conditions [*Porter*, 2012; *Perdrial et al*., 2014], which supports the hypothesis that groundwater is the dominant source of water in the Redondo system and base cations in the springs are products of primary mineral weathering reactions.

EEMT is a simple and transferable metric that quantifies energy and can predict processes within the CZ. The correlations among energy and mass inputs (EEMT) to the CZ, WTT, and mineral weathering products can provide a methodology for indirect estimations of WTT and mineral weathering products. Based on the results of this study, it is hypothesized that EEMT estimations, based on climatic variables, can be used to scale hydrological and hydrochemical response in other sites. The EEMT model has a limitation that it does not provide information how energy is distributed within the CZ and does not by itself provide a mechanistic understanding of CZ processes. However, the results of this study indicate that EEMT can be used as a tool to postulate locations of more or less intense weathering, and to identify research sites for further investigations toward mechanistic understanding of CZ processes.

5. Summary

Results from this study demonstrate the close interrelationship between landscape, hydrological, and biogeochemical processes. Our study highlights statistically significant relations between effective energy and mass transfer (EEMT) to the subsurface critical zone, WTT, and mineral weathering in springs draining catchments along a gradient of energy controlled by differences in terrain aspect around Redondo Peak, in northern New Mexico. Spring waters around Redondo Peak are dominated by Ca^+, Na^+, Si, and HCO_3^- and have an isotopic signature that indicates that they are predominantly derived from infiltration of snowmelt. Terrain aspect controls EEMT where north-facing slopes receive 25% more EEMT than south-facing slopes. Larger concentrations of total base cations and Na^+ were observed in springs with longer flow paths, larger contributing areas, and north-facing slopes. This result is consistent with longer WTT based on tritium analysis of springs draining north-facing terrains. Mineral dissolution fluxes increase with WTT, likely due to enhanced water-rock reaction, and chemical weathering consumes more atmospheric CO_2 along north-facing slopes. This study provides evidence that fluxes of energy and mass, quantified as EEMT, at the catchment scale can effectively predict short time scale (months to years) processes within the CZ structure like WTT and silicate mineral weathering. These results also suggest that basic climatic data embodied in the EEMT term can be used to scale hydrological and hydrochemical responses in other sites.

Acknowledgments
We are grateful to collaborators Chief Scientist Bob Parmenter and Research Hydrologist Scott Compton, at the Valles Caldera National Preserve. LiDAR data acquisition and processing were completed by the National Center for Airborne Laser Mapping (NCALM), funded by the National Science Foundation award EAR-0922307, and coordinated by Qinghua Guo for the Jemez River Basin and Santa Catalina Mountains Critical Zone Observatory funded by the National Science Foundation award EAR-0724958. Age dating of spring waters was supported by research grants from the University of the Pacific and a student grant from the Geological Society of America (GSA). Logistical support and/or data were provided by the NSF-supported Jemez River Basin and Santa Catalina Mountains Critical Zone Observatory (EAR-0724958 and EAR-1331408). Data access and data sharing policy are available at the Catalina-Jemez River basin Critical Zone Observatory: http://criticalzone.org/catalina-jemez/data

References

Adams, A. I., F. Goff, and D. Counce (1995), Chemical and isotopic variations of precipitation in the Los Alamos region, New Mexico, *Rep. LA-12895-MS*, Los Alamos Natl. Lab., Los Alamos, N. M.

Allison, J. D., D. S. Brown, and K. J. Novo-Gradac (1991), MINTEQA2/PRODEFA2, A geochemical assessment model for environmental systems: Version 3.0, *Rep. EPA/600/3-91/021*, Environ. Res. Lab., Off. of Res. and Dev., U.S. Environ. Prot. Agency, Athens, Ga.

Anderson, S., and W. Dietrich (2001), Chemical weathering and runoff chemistry in a steep headwater catchment, *Hydrol. Processes*, *15*, 1791–1815.

Berner, R., A. Lasaga, and R. Garrels (1983), The carbonate-silicate geochemical cycle and its effect on atmospheric carbon-dioxide over the past 100 million years, *Am. J. Sci.*, *283*, 641–683.

Berner, R. A. (1995), Chemical weathering and its effect on atmospheric CO_2 and climate, in *Chemical Weathering Rates of Silicate Minerals*, vol. 31, edited by A. F. White and S. B. Brantley, chap. 13, pp. 565–583, Mineral. Soc. of Am., Washington, D. C.

Bevington, P. R., and D. K. Robinson (1992), *Data Reduction and Error Analysis for the Physical Sciences*, 322 pp., McGraw-Hill, N. Y.

Biron, P., A. Roy, F. Courschesne, W. Hendershot, B. Cote, and J. Fyles (1999), The effects of antecedent moisture conditions on the relationship of hydrology to hydrochemistry in a small forested watershed, *Hydrol. Processes*, *13*, 1541–1555.

Brantley, S. L., M. B. Goldhaber, and K. V. Ragnarsdottir (2007), Crossing disciplines and scales to understand the Critical Zone, *Elements*, *3*, 307–314.

Bricker, O. (1986), Geochemical investigations of selected eastern-United-States watersheds affected by acid deposition, *J. Geol. Soc.*, *143*, 621–626.

Broxton, P. D., P. A. Troch, and S. W. Lyon (2009), On the role of aspect to quantify water transit times in small mountainous catchments, *Water Resour. Res.*, *45*, W08427, doi:10.1029/2008WR007438.

Buck, A. L. (1981), New equations for computing vapor pressure and enhancement factor, *J. Appl. Meteorol.*, *20*, 1527–1532.

Burns, D. A., et al. (2003), The geochemical evolution of Riparian ground water in a forested piedmont catchment, *Ground Water*, *41*, 913–925.

Buttle, J. M., P. W. Hazlett, C. D. Murray, I. F Creed, D. S. Jeffries, and R. Semkin (2001), Prediction of groundwater characteristics in forested and harvested basins during spring snowmelt using a topographic index, *Hydrol. Processes*, *15*, 3389–3407.

Campbell, D., D. Clow, G. Ingersoll, M. Mast, N. Spahr, and J. Turk (1995), Processes controlling the chemistry of two snowmelt-dominated streams in the rocky mountains, *Water Resour. Res.*, *31*, 2811–2821.

Chorover, J., et al. (2011), How water, carbon, and energy drive critical zone evolution: The Jemez-Santa Catalina critical zone observatory, *Vadose Zone J.*, *10*, 884–899.

Coop, J. D., and T. J. Givnish (2007), Spatial and temporal patterns of recent forest encroachment in montane grasslands of the Valles Caldera, New Mexico, USA, *J. Biogeogr.*, *34*, 914–927.

Daly, C., M. Halbleib, J. I. Smith, P. G. Wayne, M. K. Doggett, G. H. Taylor, J. Curtis, and P. P. Pasteris (2008), Physiographically sensitive mapping of climatological temperature and precipitation across the conterminous United States, *Int. J. Climatol.*, *28*, 2031–2064, doi: 10.1002/joc.1688.

Dokuchaev, V. V. (1967), *Selected Works of V.V. Dokuchev*, Isr. Program for Sci. Transl., Jerusalem.

Drever, J. I. (1988), *The Geochemistry of Natural Waters*, 2nd ed., Prentice Hall, Upper Saddle River, N. J.

Eastoe, C. J., C. J. Watts, M. Ploughe, and W. E. Wright (2012), Future use of tritium in mapping pre-bomb groundwater volumes, *Ground Water*, *50*, 87–93.

Ellis, S., G. Levings, L. Carter, S. Richey, and M. Radell (1993), Rio-Grande Valley, Colorado, New-Mexico, and Texas, *Water Resour. Bull.*, *29*, 617–646.

Gabet, E. J., R. Edelman, and H. Langner (2006), Hydrological controls on chemical weathering rates at the soil-bedrock interface, *Geology*, *34*, 1065–1068.

Godderis, Y., L. Francois, A. Probst, J. Schott, D. Moncoulon, D. Labat, and D. Viville (2006), Modelling weathering processes at the catchment scale: The WITCH numerical model, *Geochim. Cosmochim. Acta*, *70*, 1128–1147.

Godsey, S. E., J. W. Kirchner, and D. W. Clow (2009), Concentration-discharge relationships reflect chemostatic characteristics of US catchments, *Hydrol. Processes*, *23*, 1844–1864.

Goff, F., J. N. Gardner, S. L. Reneau, and C. J. Goff (2006), *Geologic Map of the Redondo Peak Quadrangle*, *Sandoval County*, *New Mexico*, Open File Map Ser. *OFGM-111*, scale 1:24,000, N. M. Bur. of Geol. and Miner. Resour., Socorro, N. M. [Available at http://geoinfo.nmt.edu/publications/maps/geologic/ofgm/.]

Gustafson, J. R., P. D. Brooks, N. P. Molotch, and W. C. Veatch (2010), Estimating snow sublimation using natural chemical and isotopic tracers across a gradient of solar radiation, *Water Resour. Res.*, *46*, W12511, doi:10.1029/2009WR009060.

Hooper, R., N. Christophersen, and N. Peters (1990), Modeling streamwater chemistry as a mixture of soilwater end-members—An application to the Panola Mountain Catchment, Georgia, USA, *J. Hydrol.*, *116*, 321–343.

Jenny, H. (1941), *Factors of Soil Formation: A System of Quantitative Pedology*, vol. xii, 1st ed., 281 pp., McGraw-Hill, N. Y.

Kleidon, A., E. Zehe, and H. Lin (2012), Thermodynamic limits of the critical zone and their relevance to hydropedology, in *Hydropedology*, edited by H. Lin, pp. 243–281, Elsevier.

Lieth, H. (1975), Modeling the primary productivity of the world, in *Primary Productivity of the Biosphere*, edited by H. Lieth and R. H. Whitaker, pp. 237–263, Springer, N. Y.

Liu, F., R. C. Bales, M. H. Conklin, and M. E. Conrad (2008a), Streamflow generation from snowmelt in semi-arid, seasonally snow-covered, forested catchments, Valles Caldera, New Mexico, *Water Resour. Res.*, *44*, W12443, doi:10.1029/2007WR006728.

Liu, F., R. Parmenter, P. D. Brooks, M. H. Conklin, and R. C. Bales (2008b), Seasonal and interannual variation of streamflow pathways and biogeochemical implications in semi-arid, forested catchments in Valles Caldera, New Mexico, *Ecohydrology*, *1*, 239–252.

Lybrand, R. A., and C. Rasmussen (2014), Linking soil element-mass-transfer to microscale mineral weathering across a semiarid environmental gradient, *Chem. Geol.*, *381*, 26–39.

Lyon, S. W., P. A. Troch, P. D. Broxton, N. P. Molotch, and P. D. Brooks (2008), Monitoring the timing of snowmelt and the initiation of streamflow using a distributed network of temperature/light sensors, *Ecohydrology*, *1*, 215–224.

Maher, K. (2010), The dependence of chemical weathering rates on fluid residence time, *Earth Planet. Sci. Lett.*, *294*, 101–110.

Maher, K. (2011), The role of fluid residence time and topographic scales in determining chemical fluxes from landscapes, *Earth Planet. Sci. Lett.*, *312*, 48–58.

Maher, K., and C. P. Chamberlain (2014), Hydrologic regulation of chemical weathering and the geologic carbon cycle, *Science*, *343*, 1502–1504.

Maloszewski, P., and A. Zuber (1996), Lumped parameter models for interpretation of environmental tracer data, in *Manual on Mathermatical Models in Isotope Hydrology*, pp. 9–58, Int. At. Energy Agency.
Manning, A. H., J. F. Clark, S. H. Diaz, L. K. Rademacher, S. Earman, and L. N. Plummer (2012), Evolution of groundwater age in a mountain watershed over a period of thirteen years, *J. Hydrol.*, *460-461*, 13–28.
McGlynn, B., J. McDonnell, M. Stewart, and J. Seibert (2003), On the relationships between catchment scale and streamwater mean residence time, *Hydrol. Processes*, *17*, 175–181.
McGuire, K., J. McDonnell, M. Weiler, C. Kendall, B. McGlynn, J. Welker, and J. Seibert (2005), The role of topography on catchment-scale water residence time, *Water Resour. Res.*, *41*, W05002, doi:10.1029/2004WR003657.
McGuire, K. J., and J. J. McDonnell (2006), A review and evaluation of catchment transit time modeling, *J. Hydrol.*, *330*, 543–563.
Molotch, N. P., P. D. Brooks, S. P. Burns, M. Litvak, R. K. Monson, J. R. McConnell, and K. Musselman (2009), Ecohydrological control on snowmelt partitioning in mixed-conifer sub-alpine forest, *Ecohydrology*, *2*, 129–142.
Morgenstern, U., M. K. Stewart, and R. Stenger (2010), Dating of streamwater using tritium in a post nuclear bomb pulse world: Continuous variation of mean transit time with streamflow, *Hydrol. Earth Syst. Sci.*, *14*, 2289–2301.
Mueller, M. H., R. Weingartner, and C. Alewell (2012), Relating stable isotope and geochemical data to conclude on water residence times in four small alpine headwater catchment with differing vegetation cover, *Hydrol. Earth Syst. Sci. Discuss.*, *9*, 11,005–11,048.
Muldavin, E., P. Neville, C. Jackson, and T. Neville (2006), *A Vegetation Map of Valles Caldera National Preserve, New Mexico*, vol. *59*, Nat. Heritage, N. M.
National Research Council (2001), *Basic Research Opportunities in Earth Science*, Natl. Acad. Press, Washington, D. C.
Perdrial, J. N., et al. (2014), Stream water carbon controls in seasonally snow-covered mountain catchments: Impact of inter-annual variability of water fluxes, catchment aspect and seasonal processes, *Biogeochemistry*, *118*, 273–290.
Phillips, J. D. (2009), Biological energy in landscape evolution, *Am. J. Sci.*, *309*, 271–289.
Plummer, L. N., E. C. Prestemon, and D. L. Parkhurst (1994), An interactive code (NETPATH) for modeling net geochemical reactions along a flow path, version 2.0, *U.S. Geol. Surv. Water Resour. Invest. Rep.*, 94-4169, 130 pp.
Porter, C. (2012), Solute inputs to soil and stream waters in a seasonally snow covered mountain catchment determined using Ge/Si, $^{87}Sr/^{86}Sr$ and major ion chemistry: Valles Caldera, New Mexico, MS thesis, pp. 88, Univ. of Ariz., Tucson.
Rademacher, L., J. Clark, G. Hudson, D. Erman, and N. Erman (2001), Chemical evolution of shallow groundwater as recorded by springs, Sagehen basin, Nevada County, California, *Chem. Geol.*, *179*, 37–51.
Rademacher, L., J. Clark, D. Clow, and G. Hudson (2005), Old groundwater influence on stream hydrochemistry and catchment response times in a small Sierra Nevada catchment: Sagehen Creek, California, *Water Resour. Res.*, *41*, W02004, doi:10.1029/2003WR002805.
Rasmussen, C. (2012), Thermodynamic constraints on effective energy and mass transfer and catchment function, *Hydrol. Earth Syst. Sci.*, *16*, 725–739.
Rasmussen, C., and E. L. Gallo (2013), A comparison of model and empirical measures of catchment-scale effective energy and mass transfer, *Hydrol. Earth Syst. Sci.*, *17*, 3389–3395.
Rasmussen, C., and N. J. Tabor (2007), Applying a quantitative pedogenic energy model across a range of environmental gradients, *Soil Sci. Soc. Am. J.*, *71*, 1719–1729.
Rasmussen, C., R. Southard, and W. Horwath (2005), Modeling energy inputs to predict pedogenic environments using regional environmental databases, *Soil Sci. Soc. Am. J.*, *69*, 1266–1274.
Rasmussen, C., P. A. Troch, J. Chorover, P. Brooks, J. Pelletier, and T. E. Huxman (2011), An open system framework for integrating critical zone structure and function, *Biogeochemistry*, *102*, 15–29.
Rasmussen, C., J. D. Pelletier, P. A. Troch, T. L. Swetnam, and J. Chorover (2015), Quantifying topographic and vegetation effects on the transfer of energy and mass to the critical zone, *Vadose Zone J.*, doi:10.2136/vzj2014.07.0102, in press.
Rodgers, P., C. Soulsby, and S. Waldron (2005), Stable isotope tracers as diagnostic tools in upscaling flow path understanding and residence time estimates in a mountainous mesoscale catchment, *Hydrol. Processes*, *19*, 2291–2307.
Runge, E. (1973), Soil development sequences and energy models, *Soil Sci.*, *115*, 183–193.
Scanlon, B. R. (2000), Uncertainties in estimating water fluxes and residence times using environmental traces in an arid unsaturated zone, *Water Resour. Res.*, *2*, 395–409.
Sheppard, P., A. Comrie, G. Packin, K. Angersbach, and M. Hughes (2002), The climate of the US Southwest, *Clim. Res.*, *21*, 219–238.
Smeck, N. E., E. C. A. Runge, and E. E. Mackintosh (1983), Dynamics and genetic modeling of soil systems, in *Pedogenesis and Soil Taxonomy*, edited by L. P. Wilding et al., pp. 51–81, Elsevier, N. Y.
Soulsby, C., D. Tetzlaff, S. M. Dunn, and S. Waldron (2006), Scaling up and out in runoff process understanding: Insights from nested experimental catchment studies, *Hydrol. Processes*, *20*, 2461–2465.
Stewart, M. K., U. Morgenstern, and J. J. McDonnell (2010), Truncation of stream residence time: How the use of stable isotopes has skewed our concept of streamwater age and origin, *Hydrol. Processes*, *24*, 1646–1659.
Szabo, Z., D. E. Rice, L. N. Plummer, E. Busenberg, S. Drenkard, and P. Schlosser (1996), Age dating of shallow groundwater with chlorofluorocarbons, tritium/helium 3, and flow path analysis, southern New Jersey coastal plain, *Water Resour. Res.*, *32*, 1023–1038.
Tetzlaff, D., J. Seibert, K. J. McGuire, H. Laudon, D. A. Burn, S. M. Dunn, and C. Soulsby (2009), How does landscape structure influence catchment transit time across different geomorphic provinces?, *Hydrol. Processes*, *23*, 945–953.
Vazquez-Ortega, A., et al. (2015), Rare earth elements as reactive tracers of biogeochemical weathering in forested rhyolitic terrain, *Chem. Geol.*, *391*, 19–32.
Velbel, M. (1993), Constancy of silicate mineral weathering-rate ratios between natural and experimental weathering—Implications for hydrologic control of differences in absolute rates, *Chem. Geol.*, *105*, 89–99.
Velbel, M. A., and J. R. Price (2007), Solute geochemical mass-balances and mineral weathering rates in small watersheds: Methodology, recent advances, and future directions, *Appl. Geochem.*, *22*, 1682–1700.
Vitvar, T., P. Aggarwal, and J. J. McDonnell (2005), A review of isotope applications in catchment hydrology, in *Isotopes in the Water Cycle: Past, Present and Future of a Developing Science*, edited by P. K. Aggarwal, J. Gat, and K. Froehlich, pp. 151–170, Springer, Dordrecht, Netherlands.
Volobuev, V. R. (1964), *Ecology of Soils*, Isr. Program for Sci. Transl., Jerusalem.
White, A., T. Bullen, M. Schulz, A. Blum, T. Huntington, and N. Peters (2001), Differential rates of feldspar weathering in granitic regoliths, *Geochim. Cosmochim. Acta*, *65*, 847–869.
White, A. F., and S. L. Brandley (Eds.) (1995), Chemical weathering rates of silicate minerals: An overview, in *Chemical Weathering Rates of Silicate Minerals, Reviews in Mineralogy*, vol. 31, chap. 1, pp. 1–22, Mineral. Soc. of Am., Washington, D. C.

White, A. F., and S. L. Brantley (2003), The effect of time on the weathering of silicate minerals: Why do weathering rates differ in the laboratory and field?, *Chem. Geol.*, *202*, 479–506.

Wolff, J. A., K. A. Brunstad, and J. N. Gardner (2011), Reconstruction of the most recent volcanic eruptions from the Valles caldera, New Mexico, *J. Volcanol. Geotherm. Res.*, *199*, 53–68.

Wörman et al. (2007), Fractal topography and subsurface water flows from fluvial bedforms to the continental shield, *Geophys. Res. Lett.*, *34*, L07402, doi:10.1029/2007GL029426.

Yang, X., G. A. Tang, C. C. Xiao, and F. D. Deng (2007), Terrain revised model for air temperature in mountains area based on DEMs: A case study in Yaoxian county, *J. Geogr. Sci.*, *17*, 399–408, doi:10.1007/s11442-007-0399-9.

Zapata-Rios, X., P. A. Troch, P. Broxton, J. McIntosh, C. Harman, A. Harpold, and P. D. Brooks (2012), Water storage dynamics in high elevatrion semi-arid catchments, *Geol. Soc. Am. Abstr. Programs*, *44*(6), 67.

Zapata-Rios, X. (2015), *The influence of climate and landscape on hydrological processes, vegetation dynamics, biogeochemistry and the transfer of effective energy and mass to the critical zone*, PhD. Dissertation, Univ. of Ariz., 192 pp., Tucson, Ariz.

Zuber, A., K. Rózanski, J. Kania, and R. Purtschert (2010), On some methodological problems in the use of environmental tracers to estimate hydrogeologic parameters and to calibrate flow and transport models, *Hydrogeol. J.*, *19*, 53–69, doi:10.1007/s10040-010-0655-4.